J|A|C|S
ARTICLES

Published on Web 11/25/2008

# Photochromism of an Organorhodium Dithionite Complex in the Crystalline-State: Molecular Motion of Pentamethylcyclopentadienyl Ligands Coupled to Atom Rearrangement in a Dithionite Ligand

Hidetaka Nakai,*,† Takashi Nonaka,† Yousuke Miyano,† Motohiro Mizuno,*,† Yoshiki Ozawa,*,‡ Koshiro Toriumi,‡ Nobuaki Koga,*,§ Takanori Nishioka,|| Masahiro Irie,⊥ and Kiyoshi Isobe*,†

*Department of Chemistry, Graduate School of Natural Science & Technology, Kanazawa University, Kakuma-machi, Kanazawa 920-1192, Japan, Department of Material Science, Graduate School of Material Science, University of Hyogo, 3-2-1 Kouto, Kamigori-cho, Ako-gun, Hyogo 678-1297, Japan, Graduate School of Information Science, Nagoya University, Chikusa-ku, Nagoya 464-8601, Japan, Department of Material Science, Graduate School of Science, Osaka City University, Sumiyoshi-ku Osaka 558-8585, Japan, and Department of Chemistry, Rikkyo University, 3-34-1 Nishi-Ikebukuro, Toshima-ku, Tokyo 171-8501, Japan*

Received September 9, 2008; E-mail: isobe@cacheibm.s.kanazawa-u.ac.jp

***Abstract:*** In the crystalline state, the rhodium dinuclear complex $[(RhCp^*)_2(\mu\text{-}CH_2)_2(\mu\text{-}O_2SSO_2)]$ (**1**) with a photoresponsive dithionite group ($\mu$-$O_2SSO_2$) and two pentamethylcyclopentadienyl ligands ($Cp^* = \eta^5$-$C_5Me_5$) undergoes a 100% reversible unimolecular type *T* inverse photochromism upon interconversion to $[(RhCp^*)_2(\mu\text{-}CH_2)_2(\mu\text{-}O_2SOSO)]$ (**2**). The photochromism can be followed directly by using stepwise crystal structure analysis (*Angew. Chem., Int. Ed.* **2006**, *45*, 6473). In this study, we found that the photoreaction of **1** was triggered by absorption of the 510 nm light (charge transfer band from $\sigma$(S−S) to $\sigma^*$(S−S) and $\sigma^*$(Rh−Rh) orbitals assigned by DFT calculation) and included two important processes: kinetically controlled oxygen-atom transfer to produce four stereoisomers of **2** and thermodynamically controlled isomerization between the four stereoisomers of **2** to afford the most stable isomer. Although the formation rate of the four stereoisomer products was kinetically controlled and the population of the four stereoisomers produced in the system was thermodynamically controlled, both processes were regulated by the steric hindrance between the $\mu$-$O_2SSO_2$ or $\mu$-$O_2SOSO$ ligand and the reaction cavity formed by the Cp* ligands. The cooperation of both processes achieved an intriguing stereospecific oxygen-atom rearrangement to produce only one stereoisomer of **2** at the final stage of the photoreaction at room temperature. We also determined the effect of the oxygen-atom rearrangement on the rotational motion of the two crystallographically independent Cp* ligands (parallel and perpendicular arrangement). Using variable-temperature $^{13}C$ CP/MAS NMR and quadrupolar echo solid-state $^2H$ NMR spectroscopies, before photoirradiation, the activation energies for the rotation of the parallel and perpendicular Cp* ligands in **1** were determined to be $33 \pm 3$ and $7.8 \pm 1$ kJ/mol, respectively, and after photoirradiation, in **2**, they were much lower than those in **1** ($21 \pm 2$ and $4.7 \pm 0.5$ kJ/mol, respectively). The large decrease in the activation energy for the parallel Cp* in **2** is attributed to the relaxation of molecular stress via a stereospecific oxygen-atom rearrangement, which suggests that the rotational motion of the Cp* ligands is coupled to the photochromism.

## 1. Introduction

Photochromic crystals are of considerable interest because of their potential applications in the construction of novel switching devices and materials.[1] Organic photochromic molecules, especially diarylethene derivatives, have been used to build photochromic crystals.[2] On the other hand, in the field of coordination chemistry, there are no promising molecular crystals utilizing the characteristic features of the metal complexes, and there is a lack of synthetic strategies.[3] Hence, it is still a challenge to find new photochromic crystals of metal complexes that can easily be modified chemically and to determine their photochromic reaction mechanism and dynamics. We have recently reported that a photochromic rhodium

† Kanazawa University.
‡ University of Hyogo.
§ Nagoya University.
|| Osaka City University.
⊥ Rikkyo University.

(1) (a) Irie, M.; Kobatake, S.; Horichi, M. *Science* **2001**, *291*, 1769–1772. (b) Kobatake, S.; Takami, S.; Muto, H.; Ishikawa, T.; Irie, M. *Nature* **2007**, *446*, 778–781. (c) Garcia-Garibay, M. A. *Angew. Chem., Int. Ed.* **2007**, *46*, 8945–8947.

(2) (a) Harada, J.; Uekusa, H.; Ohashi, Y. *J. Am. Chem. Soc.* **1999**, *121*, 5809–5810. (b) Yamada, T.; Kobatake, S.; Muto, K.; Irie, M. *J. Am. Chem. Soc.* **2000**, *122*, 1589–1592. (c) Yamada, T.; Kobatake, S.; Irie, M. *Bull. Chem. Soc. Jpn.* **2000**, *73*, 2179–2184. (d) Morimoto, M.; Irie, M. *Chem. Commun.* **2005**, 3895–3905. (e) Harada, J.; Nakajima, R.; Ogawa, K. *J. Am. Chem. Soc.* **2008**, *130*, 7085–7091.


10.1021/ja807150a CCC: $40.75 

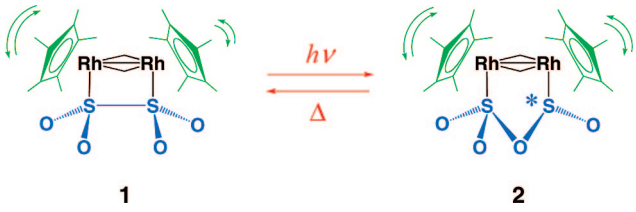


***Figure 1.*** Three processes found in the crystals: (i) fully reversible crystalline-state photochromism between $\mu$-$O_2SSO_2$ and $\mu$-$O_2SOSO$ complexes (red), (ii) reaction dynamics of the stereospecific oxygen-atom rearrangement to give the stable $\mu$-$O_2SOSO$ isomer (blue), (iii) molecular motion of the Cp* ligands coupled to the photochromic reaction (green). *: asymmetric sulfur atom.

dinuclear complex, $[(RhCp^*)_2(\mu\text{-}CH_2)_2(\mu\text{-}O_2SSO_2)]$ (**1**), with a photoresponsive dithionite group ($\mu$-$O_2SSO_2$) and two pentamethylcyclopentadienyl ligands ($Cp^* = \eta^5\text{-}C_5Me_5$) undergoes a fully reversible crystalline-state photochromic reaction with conversion to $[(RhCp^*)_2(\mu\text{-}CH_2)_2(\mu\text{-}O_2SOSO)]$ (**2**).[4] In addition, the reaction in the crystalline-state can be directly followed by using conventional single-crystal X-ray diffraction. This is a rare example of an inorganic crystalline-state photochromic system, in which the photoreaction to **2** includes two processes: a kinetically controlled oxygen-atom transfer to produce four stereoisomers of **2** and a thermodynamically controlled isomerization between the resulting four stereoisomers of **2** to afford the most stable isomer at room temperature. Both processes involve the movement of oxygen atoms. They cooperate to achieve a stereospecific oxygen-atom rearrangement (hereafter, the phrase "stereospecific oxygen-atom rearrangement" will be used when discussing the two processes mentioned above together). Our photochromic system involving intramolecular oxygen-atom insertion is not ordinary compared with the frequently reported organic photochromic systems, which involve photoinduced cyclization, cis/trans isomerization, or H atom transfer.[5] In other words, an unusual unimolecular type *T* inverse photochromism,[6] i.e., the back reaction occurs thermally, ($\lambda_{max}$(**1**) > $\lambda_{max}$(**2**)), in crystals of the dithionite compound has been observed. Working toward the elucidation of the mechanism and dynamics of this novel photochromic system, we (a) theoretically assigned UV−vis spectra of **1** and **2**, (b) performed a detailed investigation of the stereospecific oxygen-atom rearrangement process of the dithionite ligand, and (c) investigated the molecular dynamics of the Cp* ligands, which form the reaction cavities in the crystal. In this article, by using the results obtained from the studies mentioned above, we discuss the following three processes in single crystals of **1** and **2**, as shown in Figure 1: (i) fully reversible crystalline-state photochromism between **1** and **2** (red), (ii) reaction dynamics of the stereospecific oxygen-atom rearrangement to give the stable $\mu$-$O_2SOSO$ isomer (blue), and (iii) molecular motion of the Cp* ligands coupled to the photochromic reaction (green).

## 2. Results and Discussion

**2.1. Fully Reversible type *T* Inverse Photochromism in the Crystalline State.** Crystalline-state photochromism usually proceeds with interconversion ratios of less than 30% because light penetration into the bulk crystal is prohibited by the absorption of the photogenerated isomer (inner-filter effects), even if special techniques, such as two-photon excitation or linearly polarized irradiation, are used to overcome inner-filter effects.[2,3] Surprisingly, the crystalline-state photochromic system involving **1** and **2** proceeds with an interconversion ratio of ~100%, as described in the following discussion.

It is well-known that the free dithionite ion has a long S−S bond, which is cleaved readily in solution, as shown in eq 1.[7] The dithionite ion, however, may act as a bidentate ligand coordinating via the two S atoms to make dinuclear complexes.[8] In the case of the "$(RhCp^*)_2(\mu\text{-}CH_2)_2$" moiety, disulfide ($S_2^{2-}$) or thiosulfinate ($SSO_2^{2-}$) ions bridge the Rh−Rh bond via the two S atoms.[9]

$$S_2O_4^{2-} \rightleftharpoons 2SO_2^{-} \quad (1)$$

Reaction of *trans*-$[(RhCp^*)_2(\mu\text{-}CH_2)_2Cl_2]$[10] with sodium dithionite ($Na_2S_2O_4$) in methanol under $N_2$ in the dark afforded dithionite complex **1** in good yield (72%) as a reddish brown powder. Crystals of **1** were grown from a mixture of ethyl acetate and methylene chloride at room temperature. While irradiating with light from a xenon lamp (300 W, 385−740 nm) for 3 h, the red-orange crystals (approximate crystal size: 0.1 × 0.1 × 0.1 mm) of **1** change to yellow-orange crystals of **2**. The solid-state molecular structures of **1** and **2** were determined by using X-ray diffraction analysis and are shown in Figure 2. The $\mu$-$O_2SSO_2$ ligand in **1** is coordinated parallel to the Rh−Rh bond and has a weak S−S bond of 2.330(2) Å. To the best of our knowledge, this is the first example of a "side−on" type coordination mode for the dithionite ion. Complex **2** also contains a new type of oxysulfur species, $O_2SOSO$, in which an oxygen atom bridges the two S atoms. One S atom has two terminal O atoms, whereas the other has only one terminal O atom and is asymmetric. Although **2** has an asymmetric sulfur atom (S2), there are pairs of enantiomers in one single crystal of **2** because of the centrosymmetric space group $P2_1/n$. $O_2SOSO$ compounds have been thought to be important, but unstable, intermediates in the oxidation of disulfide compounds

(3) (a) Boldyreva, E. V. *Mol. Cryst. Liq. Cryst.* **1994**, *242*, 17–52. (b) Rack, J. J.; Winkler, J. R.; Gray, H. B. *J. Am. Chem. Soc.* **2001**, *123*, 2432–2433. (c) Nishimura, H.; Matsushita, N. *Chem. Lett.* **2002**, 930–931. (d) Coppens, P.; Novozhilova, I.; Kovalevsky, A. *Chem. Rev.* **2002**, *102*, 861–883. (e) Kovalevsky, A. Y.; Bagley, K. A.; Cole, J. M.; Coppens, P. *Inorg. Chem.* **2003**, *42*, 140–147. (f) Niibayashi, S.; Matsubara, K.; Haga, M.; Nagashima, H. *Organometallics* **2004**, *23*, 635–646.
(4) Nakai, H.; Mizuno, M.; Nishioka, T.; Koga, N.; Shiomi, K.; Miyano, Y.; Irie, M.; Breedlove, B. K.; Kinoshita, I.; Hayashi, Y.; Ozawa, Y.; Yonezawa, T.; Toriumi, K.; Isobe, K. *Angew. Chem., Int. Ed.* **2006**, *45*, 6473–6476.
(5) (a) Brown, G. H., Ed. *Photochromism*; Wiley Interscience: New York, 1971. (b) Irie, M., Ed. *Chem. Rev.* **2000**, *100* (Photochromism: Memories and Switches, Special thematic issue 5). (c) Dürr, H., Bouas-Laurent, H., Eds. *Photochromism: Molecules and Systems*; Elsevier: Amsterdam, 2003.
(6) Bouas-Laurent, H.; Dürr, H. *Pure Appl. Chem.* **2001**, *73*, 639–665.
(7) (a) Mishra, S. P.; Symons, M. C. R. *J. Chem. Soc., Dalton Trans.* **1994**, 1271–1274. (b) Cotton, F. A.; Wilkinson, G.; Murillo, C. A.; Bochmann, M. *Advanced Inorganic Chemistry*, 6th edition; John Wiley & Sons, Inc.: New York, 1999; pp 527–528.
(8) (a) Tennent, N. H.; Su, S. R.; Poffenberger, C. A.; Wojcicki, A. *J. Organomet. Chem.* **1975**, *102*, C46−C48. (b) Kubas, G. J.; Wasserman, H. J.; Ryan, R. R. *Organometallics* **1985**, *4*, 2012–2021. (c) Matsumoto, K.; Koyama, T.; Koide, Y. *J. Am. Chem. Soc.* **1999**, *121*, 10913–10923.
(9) (a) Nishioka, T.; Nakamura, S.; Kaneko, Y.; Suzuki, T.; Kinoshita, I.; Kiyooka, S.; Isobe, K. *Chem. Lett.* **1996**, 911–912. (b) Shiomi, K.; Breedlove, B. K.; Kitayama, H.; Nishioka, T.; Kinoshita, I.; Koga, N.; Isobe, K. *Chem. Commun.* **2002**, 1756–1757. (c) Nishioka, T.; Kitayama, H.; Breedlove, B. K.; Shiomi, K.; Kinoshita, I.; Isobe, K. *Inorg. Chem.* **2004**, *43*, 5688–5697.
(10) Isobe, K.; Okeya, S.; Meanwell, N. J.; Smith, A. J.; Adams, H.; Maitlis, P. M. *J. Chem. Soc., Dalton Trans.* **1984**, 1215–1221.

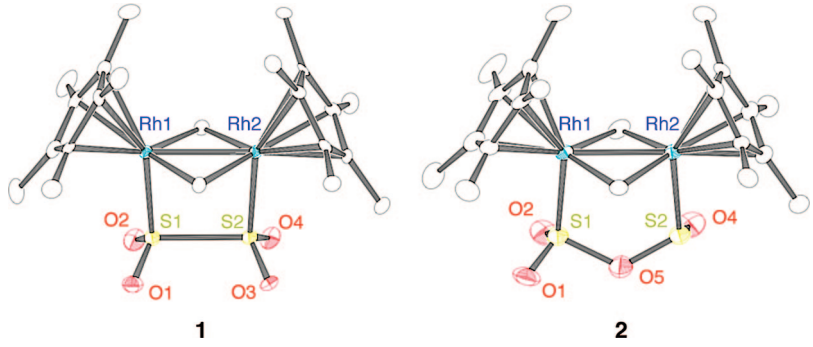


***Figure 2.*** ORTEP drawings of **1** (left) and **2** (right) with 50% probability ellipsoids. Hydrogen atoms are omitted for clarity. Selected bond lengths (Å) and angles (deg) for **1**: Rh1−Rh2 2.6224(5), Rh1−S1 2.279(1), Rh2−S2 2.277(1), S1−S2 2.330(2), S1−O1 1.462(5), S1−O2 1.459(4), S2−O3 1.467(5), S2−O4 1.464(4), Rh2−Rh1−S1 86.63(4), Rh1−Rh2−S2 86.00(3), Rh1−S1−S2 93.29(6) Rh2−S2−S1 94.06(5). Selected bond lengths (Å) and angles (deg) for **2**: Rh1−Rh2 2.6257(6), Rh1−S1 2.270(2), Rh2−S2 2.285(2), S1−O1 1.445(7), S1−O2 1.440(6), S1−O5 1.709(5), S2−O5 1.636(6), S2−O4 1.486(6), S1···S2 2.964(3), Rh2−Rh1−S1 94.15(5), Rh1−Rh2−S2 94.35(5), Rh1−S1−O5 107.9(2), Rh2−S2−O5 107.8(2), S1−O5−S2 124.7(3). Adapted from ref 4.

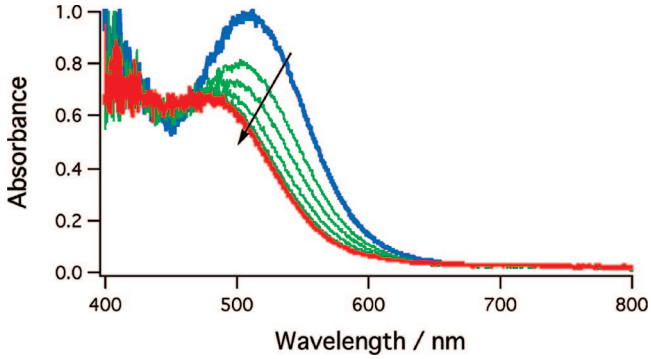


***Figure 3.*** Irradiation time-resolved UV−vis spectra of **1** (blue) to **2** (red) in a microcrystalline powder film. Adapted from ref 4.

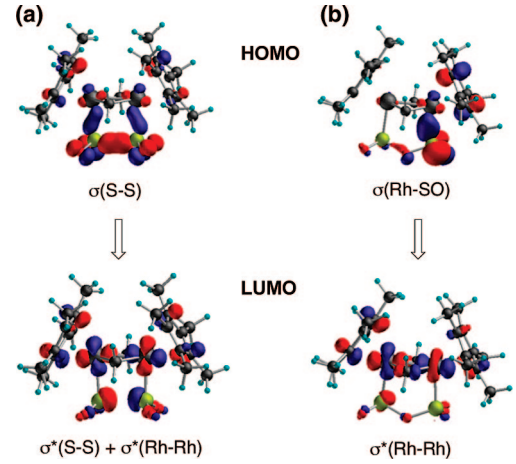


***Figure 4.*** HOMO−LUMO transition dominant in the lowest excited-state for (a) **1** and (b) **2** (clarified by time-dependent DFT calculations).

to $SO_3^{2-}$ and $SO_4^{2-}$ and has only been studied theoretically.[11] The S1−O5 and S2−O5 bonds of the bridging moiety in **2** differ significantly in length (S1−O5: 1.709(5), S2−O5: 1.636(6) Å), and the latter has double-bond character. The $O_2SOSO$ moiety in complex **2** is stabilized by the side-on type coordination mode and the electron rich Rh−Rh bond.

UV−vis absorption spectra were acquired on the same sample before and after irradiation. Figure 3 shows the UV−vis spectral change during the conversion from **1** to **2** in a microcrystalline powder film. A hypsochromic (blue) shift of $\lambda_{max}$ from 510 to 475 nm, which is characteristic of inverse photochromism, was observed. More importantly, the absorption coefficient of $\lambda_{max}$ for **2** is about one-third of that for **1**, which is very rare. Thus, the light is able to pass more easily through crystals of **1**, and the photoreaction proceeds with an interconversion ratio of almost 100%.

The nature of the absorption band in the UV−vis spectra of **1** and **2** was examined by using B3LYP hybrid DFT and time-dependent DFT (TD-DFT) calculations.[12] The TD-DFT calculations could be used qualitatively to reproduce the observed blue-shift. The calculated $\lambda_{max}$ value for **1** was 540 nm, whereas that for **2** was 526 nm. In addition, the corresponding oscillator strength for **2** (0.0437) was calculated to be half of that for **1** (0.0861). The dominant configuration for these excitations was determined to be a HOMO−LUMO transition. Figure 4 shows the HOMO and LUMO for the ground-state of **1** and **2**. Since the HOMO and LUMO of **1** extends over the same region, the larger overlap density results in a larger oscillator strength. From a visual inspection of Figure 4, we assigned the absorption band at 510 nm in the spectrum of **1** to be the charge transfer (CT) band from the $\sigma$(S−S) to the $\sigma^*$(S−S) and $\sigma^*$(Rh−Rh) orbitals and that at 475 nm in the spectrum of **2** to be the CT band from the $\sigma$(Rh−SO) to the $\sigma^*$(Rh−Rh) orbitals. These results indicate that the initial step of the atom rearrangement from **1** to **2** is the light-induced S−S bond cleavage of **1** and that the back reaction from **2** to **1** does not occur photochemically upon irradiation at 475 nm (i.e., photochemical reactivity of the light-induced isomer **2** is low).

When crystals of **2** were left in the dark for three weeks at room temperature, a back reaction took place to regenerate completely crystals of **1**. Differential scanning calorimetry (DSC) analysis of **2** showed that the back reaction was exothermic with liberation of about 19 kJ/mol of heat. The S−O−S bonding character in the $O_2SOSO$ ligand in **2** indicates that selective cleavage of the weak S1−O5 bond is the lowest-energy path for returning to complex **1** and may be the only path for isomerization to **1**. The photochromic system involving **1** and **2** was repeatable in the crystalline state. In contrast, in solution, irradiation of **1** caused an oxidation reaction with atmospheric oxygen to occur, resulting in a mixture of **2** and further oxidation products, such as $[(RhCp^*)_2(\mu\text{-}CH_2)_2(\mu\text{-}SO_3)]$

(11) Lacombe, S.; Loudet, M.; Dargelos, A.; Robert-Banchereau, E. *J. Org. Chem.* **1998**, *63*, 2281–2291.
(12) Frisch, M. J.; et al. Gaussian 03, revision C.02; Gaussian, Inc.: Wallingford, CT, 2004.

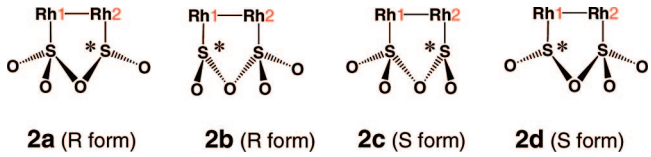


***Figure 5.*** Stereoisomers of **2**. The Cp* and $\mu$-$CH_2$ ligands are omitted for clarity. Adapted from ref 4.

and $[(RhCp^*)_2(\mu\text{-}CH_2)_2(\mu\text{-}SO_4)]$. The quantum yield of the photoreaction in acetonitrile without $O_2$ was $0.14 \pm 0.01$ at 509 nm. Further results on the photoreactivity of **1** in solution will be published elsewhere.

**2.2. Dynamics of Crystalline-State Photochromic Reaction.** Although some crystalline-state reactions, including photochromic reactions, have been investigated based on crystal structures before and after the reactions, little is known about the dynamics of the molecular structural changes in crystalline-state reactions.[3d,4,13]

The unique full reversibility of the crystalline-state photochromic system involving **1** and **2** can be utilized in clarifying the reaction dynamics by using spectroscopic methods and other techniques. For instance, NMR and FT-IR spectroscopic methods are very useful for determining the interconversion ratios between **1** and **2**. In addition, the crystalline-state photochromic processes, including the kinetically controlled oxygen-atom transfer and thermodynamically controlled isomerization, can be followed directly by using conventional single crystal X-ray diffraction.[4] During the photoreaction from **1** to **2**, positional disorder and occupancy changes in the oxygen atoms with irradiation time were observed in the X-ray diffraction analyses. In contrast, the thermal back reaction did not show any disorder phenomena except for that due to the formation of **1**. This observation is consistent with the S−O−S bonding character of the $O_2$SOSO ligand in **2**, of which the S1−O5 bond length is significantly longer than the S2−O5 bond length (*vide ante*), which causes a regiospecific S−O bond cleavage.

A careful analysis of the time dependence of the positional disorder and the changes in the occupancy of the oxygen atoms during photoreaction (two halogen lamps, 12 V, 75 W) at 20 °C indicated that at the initial stage of the reaction (unconverted starting complex exists at $72 \pm 1\%$) four species, **2a**−**d**, were generated with respective yields of 10, 8, 5, and $5 \pm 1\%$ (Figure 5 and Figure 6a).

Species **2a**−**d** that caused the positional disorder were stereoisomers of **2** in the crystal. Although the crystal had mirror images of **2a**−**d** as a set, in the present treatment only one asymmetric unit in the crystal was considered. Isomers **2a** and **2c** are a pair of enantiomers, **2a** and **2b** are identical species but differ orientationally in the cavity, and **2c** and **2d** are also identical but differ in orientation. The oxygen atoms in **2a**−**d** had only a *trans* arrangement. We found no evidence for the existence of the *cis*-isomer (Figure 7) in the disorder analysis, and the DFT calculations also indicated that the *cis*-isomer was 2.3 kcal/mol less stable than the *trans*-isomer.

When the photoreaction was at $93 \pm 1\%$, the yields of **2a**–**d** were 62, 25, 2, and $4 \pm 1\%$, respectively. At the final stage, only **2a** was formed, and the positional disorder was barely

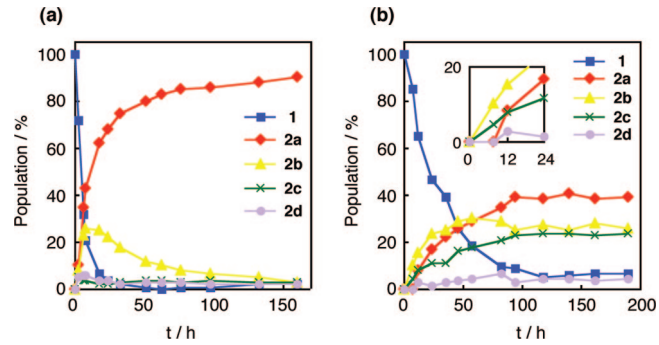


***Figure 6.*** Changes in the population of the photochemically generated isomers with irradiation time at (a) 20 °C and (b) −163 °C. X-ray crystallographic data were recorded at −163 °C. Crystal sizes: $0.10 \times 0.08 \times 0.06$ mm$^3$ for (a) and $0.12 \times 0.10 \times 0.05$ mm$^3$ for (b). (Inset) Magnification of the initial stage of the reaction. All the plots except for 0 h data have ± 1% errors due to esd's (estimated standard deviation) of the occupancy factors of the oxygen atoms.

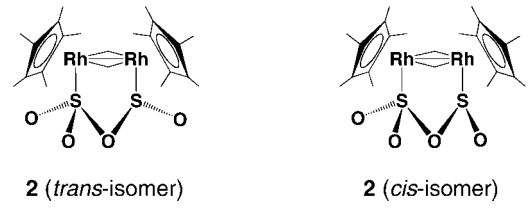


***Figure 7.*** *Trans*- and *cis*-isomers of **2**.

observed. This disappearance means that the thermodynamically unstable $\mu$-$O_2$SOSO species, **2b**−**d**, generated in the crystal, convert to the most stable species **2a**.

In order to determine a detailed mechanism for the isomerization to **2a**, we carried out several low temperature experiments after our short communication[4] was published and obtained the following information concerning the oxygen-atom rearrangement process of the dithionite ligand. The reaction at −163 °C clearly had a different reaction rate and population from those at 20 °C (Figure 6b). The irradiation time dependence of the population of the light-induced isomers at −163 °C showed that **2a**, which is the most stable product, was not produced in the highest population in the initial stage of the reaction. In the initial stage of the reaction (unconverted starting complex exists at $65 \pm 1\%$), **2a**−**d** were present in respective yields of 8,16, 8, and $3 \pm 1\%$ (Figure 6b, inset). There were no obvious conversions among the isomers at −163 °C. These results strongly indicate that, at −163 °C, the kinetically controlled reaction predominantly takes place in the initial stage of the reaction. In this article, the phrase "kinetically controlled reaction" is used for the isomerization from **1** to **2** to produce four stereoisomers **2a**−**d** based on the kinetic ease for the oxygen atom transfer and the phrase "thermodynamically controlled reaction" is used for the isomerization of between the four stereoisomers of **2** to afford the most stable isomer **2a**.

In order to study the thermal conversions among the isomers of **2**, the time dependence of the population of the isomers generated at −163 °C after 190 h of irradiation was examined at 20 °C in the dark (Figure 8). The increase in the population of **2a** (+22%) with the corresponding decrease in the population of **2c** (−22%) showed that isomer **2c** directly transformed into **2a** without irradiation. The unchanged populations of **2b** and **2d** confirmed that the direct thermal conversion process of **2b** (or **2d**) into **2a** did not occur at 20 °C. These results are consistent with the structural relationship between the isomers

(13) (a) Ramamurthy, V.; Venkatesan, K. *Chem. Rev.* **1987**, *87*, 433–481. (b) Desiraju, G. R., Ed. *Crystal Engineering: The Design of Organic Solids*; Elsevier: Amsterdam, 1989. (c) Ohashi, Y. *Acta Crystallogr.* **1998**, *A54*, 842–849. (d) Braga, D.; Grepioni, F. *Angew. Chem., Int. Ed.* **2004**, *43*, 4002–4011. (e) Kawano, M.; Fujita, M. *Coord. Chem. Rev.* **2007**, *251*, 2592–2605.

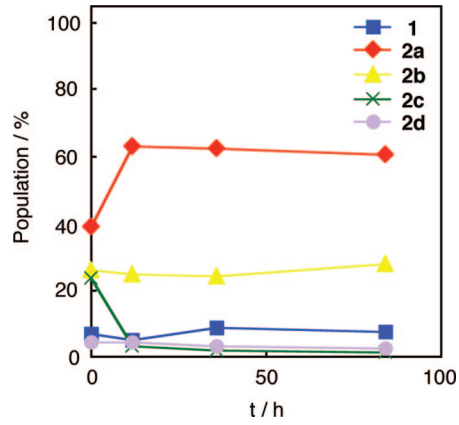


***Figure 8.*** Time dependence of the population of the light-induced isomers generated at −163 °C for 190 h irradiation. The back reaction scarcely occurs. The experiments were carried out at 20 °C. Crystal size: 0.12 × 0.10 × 0.05 mm$^3$. All the plots have ± 1% errors due to esd's (estimated standard deviation) of the occupancy factors of the oxygen atoms.

in the crystal. The transformation from **2c** to **2a** can occur via a simple flip of the bridging and terminal oxygen atoms of **2c**. Since the direct photochemical transformation from **2b** (or **2d**) to **2a** can be ignored based on the photoreaction results at −163 °C and the photoabsorption properties of **2**, as shown in Figure 4b, the conversion of **2b** (or **2d**) to **2a** is a purely photochromic process of **2b** (or **2d**) → **1** → **2a**; the reaction from **2b** (or **2d**) to **1** does not take place photochemically, but thermally because of the type *T* inverse photochromism of **1** (*vide ante*).

Thus, the oxygen transfer was specific during the photoreaction at 20 °C because **2a**, which is thermodynamically favorable, accumulates through direct thermal conversion from **2c** to **2a** and the repetitive photochromic process (**2b** (or **2d**) → **1** → **2a**). Although the disappearance rate of **2b** in Figure 6a (less than 100 h) seems considerably faster than that expected for the thermal back reaction at 20 °C (**2** → **1**, 3 weeks), the difference is reasonable because **2b** is unstable compared to **2a**, which means that **2b** converts faster to **1** than **2a** does. In addition, in the experiment to acquire the data in Figure 6a, the sample crystal was exposed to thermic rays during irradiation.

We investigated the possible causes for the selectivity of the photoreaction in the initial stage at −163 °C. Since the crystals of **1** and **2** have the same space group and molecular arrangement, by comparing certain molecules in the unit cell of **1** with those of **2**, it can be readily seen which terminal oxygen atom in the $\mu$-$O_2SSO_2$ ligand of **1** becomes the bridging oxygen in **2** (Figure 9). In the case of **2a**, atom O3 was transferred. In the $\mu$-$O_2SSO_2$ ligand, the four oxygen atoms are stereochemically nonequivalent in the cavity formed by the six Cp* ligands. Based on this situation, they do not have an equal chance to undergo transfer. As shown in Figure 10, atom O3 is the most congested by the methyl groups of the Cp* ligands. Thus, migration of atom O3 is more difficult than that of the other O atoms. We believe that this is the origin of the kinetically controlled reaction at −163 °C. Since **2a** is the kinetically unfavorable product, the initial population of the products at −163 °C reflects the selectivity based on the shape of the cavity in the crystal of **1** (topochemical principle[14]). Thus, the oxygen atom in **2a** is not stereochemically congested in the cavity, which makes **2a** thermodynamically favorable, as mentioned before. This stereospecific oxygen atom migration induces a change in the dynamic behavior of the Cp* rings in the crystal, which will be described in the next section.

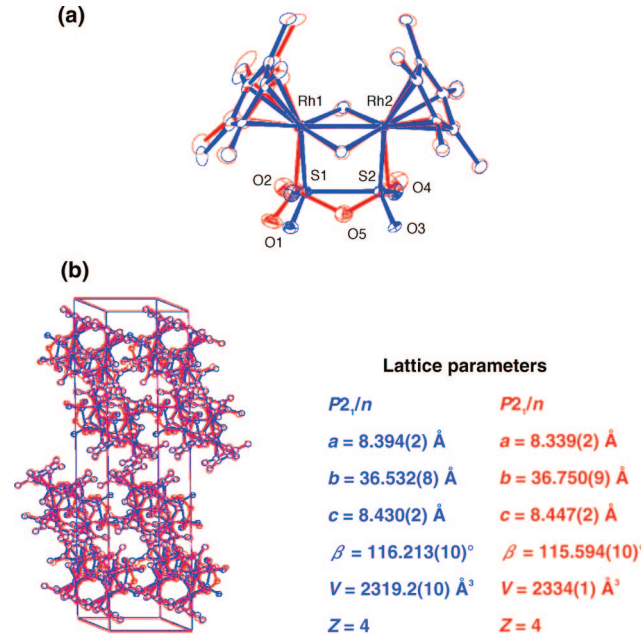


***Figure 9.*** Superimposition of (a) crystal structures and (b) unit cells of **1** (blue) and **2** (red). Adapted from ref 4.

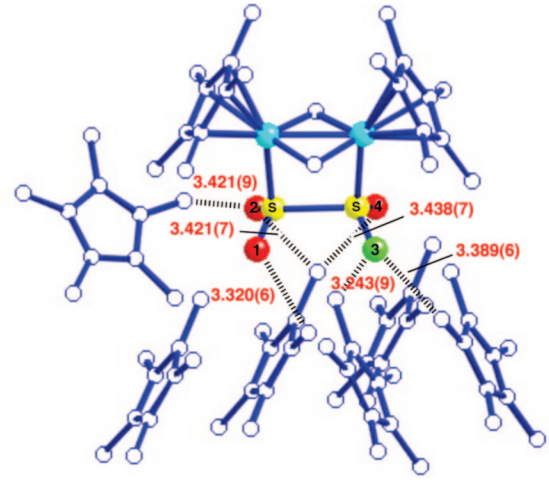


***Figure 10.*** Reaction cavity around the $\mu$-$O_2SSO_2$ unit surrounded by the Cp* ligands of neighboring molecules in the crystal of **1**.

**2.3. Dynamics of the Cp* Ligands: Molecular Motion Coupled to the Photochromic Reaction.** It is well-known that flat disklike ligands, such as $\eta^5$-$C_5H_5$ (Cp) and Cp*, can undergo $2\pi/5$ jumping motions, i.e., "rotational motion", around the ligand−metal coordination $C_5$ axis in the crystal.[15] In our system, the crystalline-state sterospecific oxygen-atom rearrangement proceeds in the reaction cavities formed by the Cp* ligands. Hence, the rearrangement may have some influence on the motion of the Cp* ligands. We performed variable temperature (VT) solid-state NMR measurements to investigate the dynamic behavior of the Cp* ligands by using protio- and deuterio-complexes **1** and **2** and found the rotational motion of the Cp* ligands was

(14) (a) Cohen, M. D.; Schmidt, G. M. J. *J. Chem. Soc.* **1964**, 1996–2000. (b) Schmidt, G. M. J. *Pure Appl. Chem.* **1971**, *27*, 647–678.

(15) (a) Bryan, R. F.; Greene, P. T.; Newlands, M. J.; Field, D. S. *J. Chem. Soc. A* **1970**, 3068–3074. (b) Braga, D. *Chem. Rev.* **1992**, *92*, 633–665.

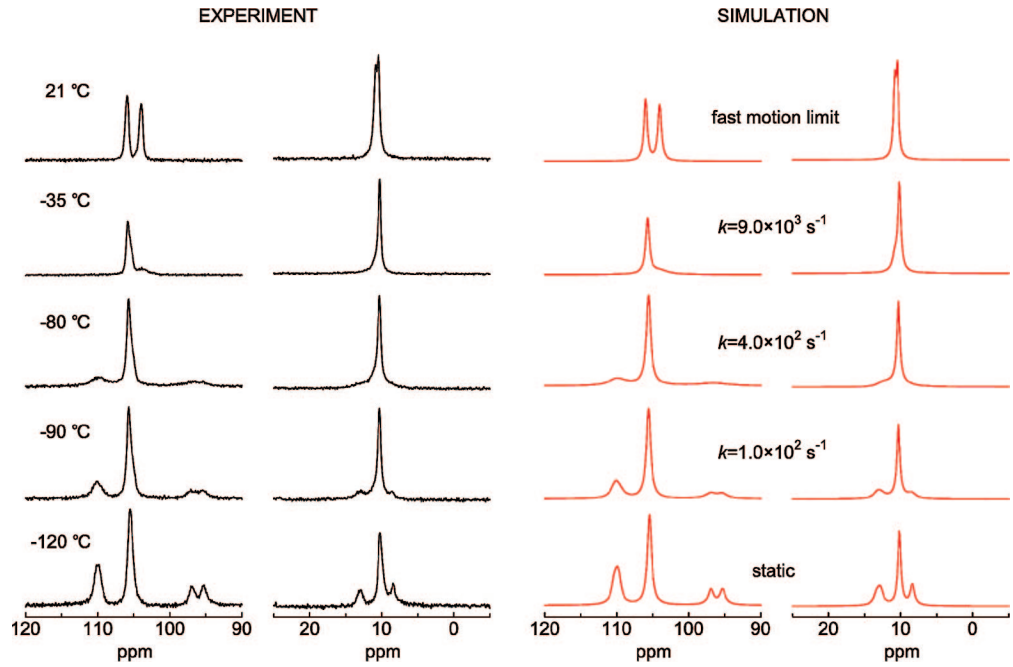


***Figure 11.*** Experimental (left) and simulated (right) Cp* ring and methyl signals in solid-state $^{13}C$ CP/MAS NMR spectra of **1**. The jump rates of the Cp* rings ($k$) are indicated.

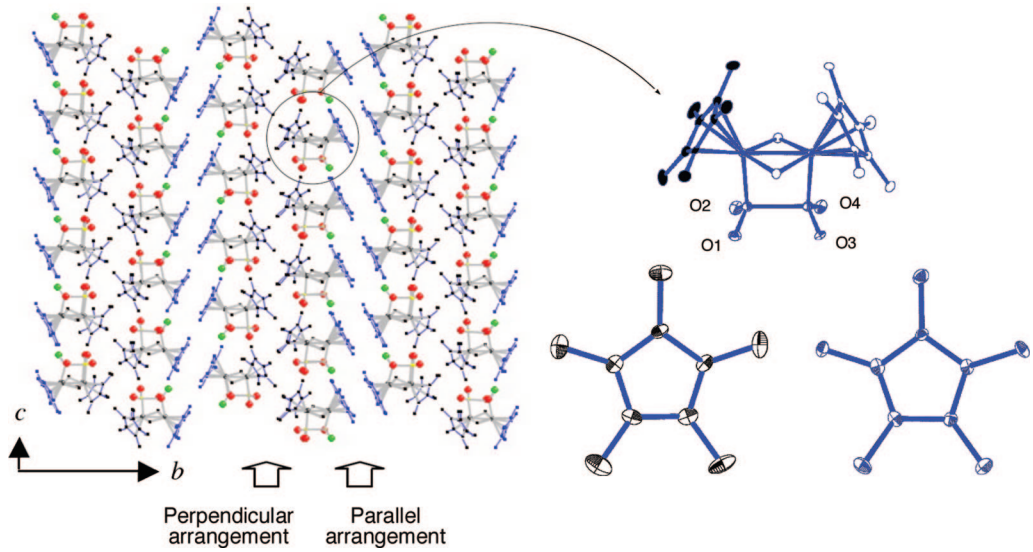


***Figure 12.*** Packing diagram of **1** and the thermal ellipsoids (50% probability) of C-atoms of two crystallographically independent Cp* rings in **1**. Red: oxygen atoms. Green: atom O3.

coupled to the photochromic reaction, which has not been reported previously to our knowledge.

In the solid-state $^{13}C$ CP/MAS NMR spectrum of the Cp* ligands in the crystals of **1** at 21 °C (Figure 11) there were two methyl carbon signals at 10.5 and 10.8 ppm and two ring carbon signals at 104.0 and 106.0 ppm, reflecting the presence of two crystallographically independent Cp* ligands (in chloroform solution only one methyl and one ring carbon signal appeared at 9.6 and 104.1 ppm, respectively). Both the 10.8 and 104.0 ppm signals showed a significant temperature dependence, whereas the signals at 10.5 and 106.0 ppm did not. As shown in Figure 11, spectra of the former pair of signals were simulated with a FORTRAN program written in-house using a model that assumes a five-site jump of the Cp* ring around the $C_5$ axis. From an Arrhenius plot of the data, the activation energy was determined to be 30 ± 3 kJ/mol. An activation energy of less than 17 kJ/mol was estimated by using line width analysis ($k \geq 10^5$ $s^{-1}$ at −120 °C) of the latter pair of signals (10.5 and 106.0 ppm at 21 °C).

It has been reported that, in X-ray analysis, the extent and direction of the atomic displacements, corresponding to the shapes of the thermal ellipsoids, contain information about dynamic processes in the solid state.[15] As shown in Figure 12, the shapes of the thermal ellipsoids of the C-atoms of the two crystallographically independent Cp* rings, which are in parallel and perpendicular arrangements in **1**, at −163 °C, were quite different from each other due to the thermal motion of Cp* rings, which are related to their activation energies.

These ellipsoid patterns clearly showed that the parallel Cp* ligands had a large activation energy for the slow jumping

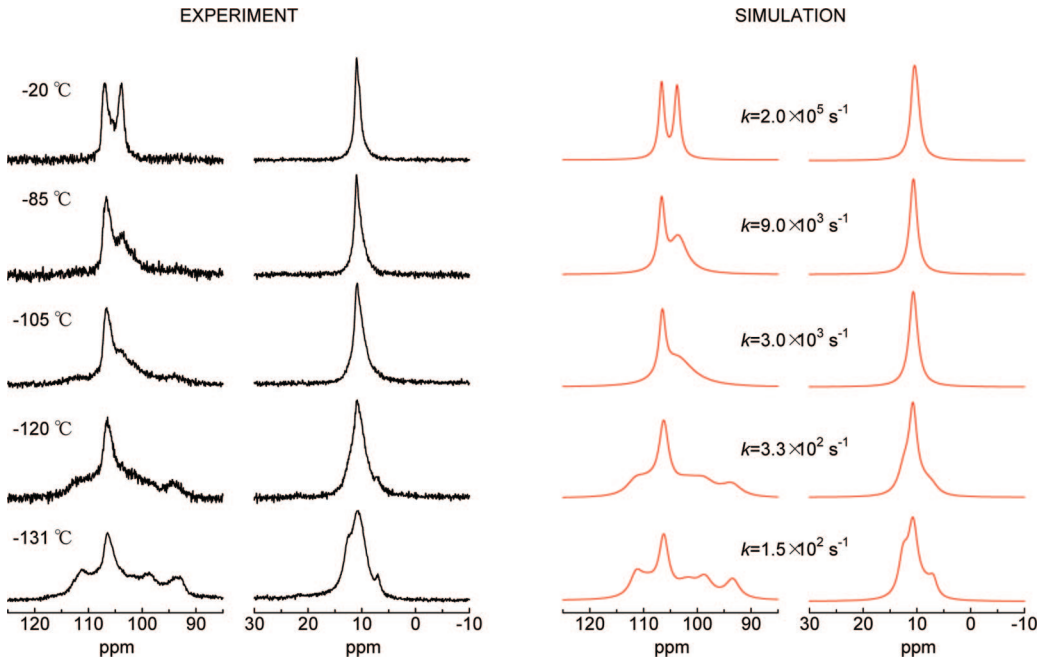


***Figure 13.*** Experimental (left) and simulated (right) Cp* ring and methyl signals in solid-state CP/MAS $^{13}$C NMR spectra of **2**. The jump rates of the Cp* rings ($k$) are indicated.

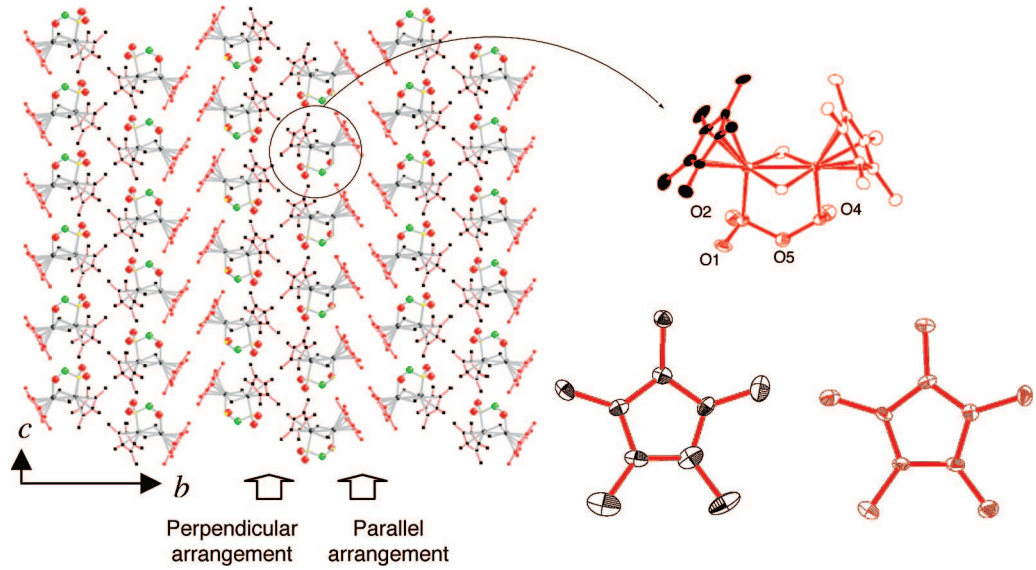


***Figure 14.*** Packing diagram of **2** and the thermal ellipsoids (50% probability) of C-atoms of two crystallographically independent Cp* rings in **2**. Red: oxygen atoms. Green: atom O5 (transferd from O3 position).

motion. In the crystal of **1**, the parallel Cp* ligands are the closest to the terminal O3 atoms and the rings in two adjacent molecules are staggered (two parallel Cp* rings form an intermolecular staggered arrangement). Thus, the motion of the parallel Cp* ligands in **1** is restricted by the steric hindrance of atom O3 in addition to the intermolecular staggered form itself. In other words, complex **1** has molecular stress in the crystal. Interestingly, in complex **2**, which has an analogous Cp* arrangement to that of **1**, the activation energy was determined to be 20 ± 2 kJ/mol for the rotational motion of the parallel Cp* rings and is much lower than that in **1** (Figure 13 and Figure 14). The smaller activation energy for the rotational motion arises from an easing of the molecular stress in crystals of **1** via the photoreaction, in which transfer of atom O3 and an increase in the packing distance of the parallel Cp* rings (3.5793(20) and 3.6323(25) Å in crystal **1** and **2**, respectively) occur. In this way, atom O3 controls the rotational motion of the Cp* ligands in the crystal. Although the activation energy was estimated to be less than 10 kJ/mol for the motion of the perpendicular Cp* ligands in **2** by using line width analysis of the VT $^{13}$C CP/MAS NMR spectra, accurate activation energies for the motion of the perpendicular Cp* ligands in **1** and **2** could not be obtained by using $^{13}$C CP/MAS NMR spectroscopy.

To confirm the results obtained from $^{13}$C CP/MAS NMR spectroscopy and to clarify the dynamic behavior of the perpendicular Cp* ligands in our crystalline-state photochromic system, we synthesized the deuterated analogue $[(RhCp^{*d15})_2(\mu\text{-}CH_2)_2(\mu\text{-}O_2SSO_2)]$ (**1**-$d_{30}$) ($Cp^{*d15} = \eta^5\text{-}C_5(CD_3)_5$) and analyzed the molecular motion of the Cp* ligands by using quadrupolar echo $^2$H NMR spectroscopy, which is a very powerful method

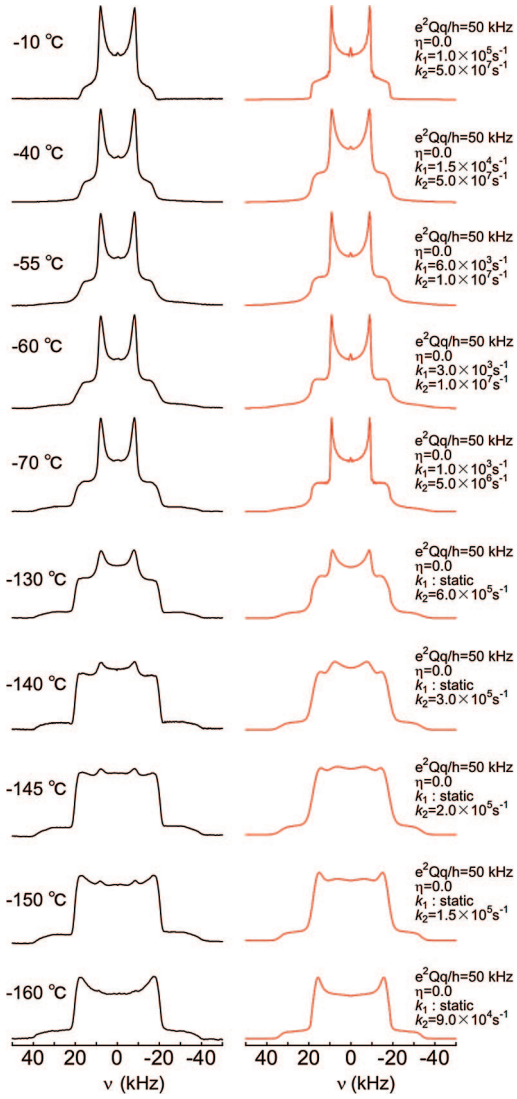


***Figure 15.*** Experimental (left) and simulated (right) solid-state $^2$H NMR spectra of **1**-$d_{30}$. The jump rates of the Cp* rings ($k$), the nuclear quadrupole coupling constants ($e^2Qq/h$), and the asymmetry parameters ($\eta$) are indicated.

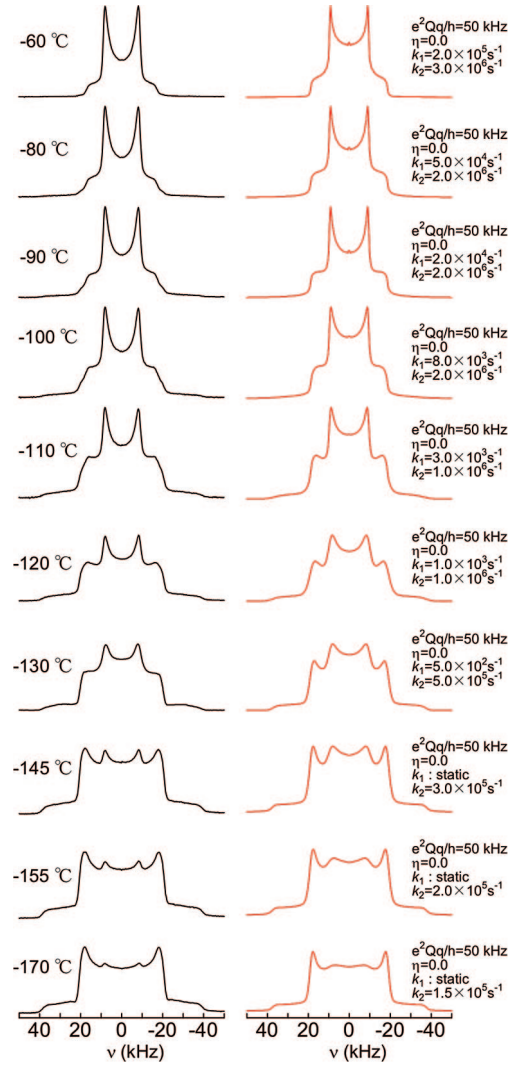


***Figure 16.*** Experimental (left) and simulated (right) solid-state $^2$H NMR spectra of **2**-$d_{30}$. The jump rates of the Cp* rings ($k$), the nuclear quadrupole coupling constants ($e^2Qq/h$), and the asymmetry parameters ($\eta$) are indicated.

for determining internal molecular dynamics in the solid state.[16] It was confirmed that the crystal structure, crystalline-state reactivity, and quantum yield of a solution of **1**-$d_{30}$ were identical to those of **1**. VT $^2$H NMR spectra of **1**-$d_{30}$ recorded in the temperature range of −10 to −160 °C are shown in Figure 15. The line shape changed significantly with the temperature.

The observed spectra were simulated by using an in-house FORTRAN program with two independent models that assume a five-site jump of the Cp* ring around the $C_5$ axis, a nuclear quadrupolar coupling constant ($e^2Qq/h$) of 50 kHz, and exchange rates between 10 kHz and 10 MHz. From an Arrhenius plot of the data, the activation energies were determined to be 33 ± 3 and 7.8 ± 1 kJ/mol for motion of the parallel and perpendicular Cp* ligands, respectively, in the crystal of **1**-$d_{30}$. Using a similar analysis of the VT $^2$H NMR data obtained from the crystal of **2**-$d_{30}$, the activation energies for the motion of the parallel and perpendicular Cp* ligands were determined to be 21 ± 2 and 4.7 ± 0.5 kJ/mol, respectively (Figure 16). The values obtained for the motion of the parallel Cp* ligand in the crystal of **1**-$d_{30}$ and **2**-$d_{30}$ are consistent with those determined from the $^{13}$C CP/MAS NMR data of **1** and **2**. Thus, the activation energies for the motion of the Cp* ligands in **1** and **2** were unequivocally determined by using VT solid-state $^2$H NMR analyses. The results show that the molecular motion of the Cp* ligands is coupled to the photochromic reaction (atom rearrangement of the dithionite ligand). This strongly indicates that the dynamic behavior of the Cp* ligands assists the crystalline-state reaction to proceed maintaining the single-crystal integrity and forming only one enantiomeric pair of the $\mu$-$O_2$SOSO complex at the final stage of the photoreaction at 20 °C. The activation energy change of 12 kJ/mol (subtract 21 from 33) for the motion of the parallel Cp* ligands in the photoreaction from **1** to **2** is much greater than that of 3.1 kJ/mol (subtract 4.7 from 7.8) for the motion of the perpendicular Cp* ligands. The results indicate that the relaxation of the molecular stress by the stereospecific rearrangement of atom O3 and by expansion of the distance between the parallel Cp* rings in the crystal of **1** is the main

(16) (a) Garcia-Garibay, M. A. *Proc. Natl. Acad. Sci. U. S. A.* **2005**, *102*, 10771–10776. (b) Khuong, T.-A. V.; Nuñez, J. E.; Godinez, C. E.; Garcia-Garibay, M. A. *Acc. Chem. Res.* **2006**, *39*, 413–422. (c) Horike, S.; Matsuda, R.; Tanaka, D.; Matsubara, S.; Mizuno, M.; Endo, K.; Kitagawa, S. *Angew. Chem., Int. Ed.* **2006**, *45*, 7226–7230.

contribution to the reduction in the activation energy for the motion of the parallel Cp* ligands.

## 3. Conclusion

In conclusion, we showed that a rhodium dinuclear complex **1** with two Cp* rings and a photoreactive dithionite ligand undergoes a fully reversible crystalline-state photochromic reaction. This photochromic process is a repetitive crystalline-state reaction accompanied by (i) "*expansion—shrinkage*" sequences of the crystal lattice with a change in density (about 1% change in volume), (ii) "*gain—loss*" sequences of the asymmetric center, although the space group remains $P2_1/n$, (iii) "*lock—unlock*" sequences by the oxygen atom (O3) that controls the rotational motion of the Cp* ligands in the crystal, in addition to the color change. These essential processes for switching functions occur in a single crystal and are closely connected to one another. Thus, a feedback loop consisting of a light, chemical, kinetic, and thermal energy sequence was observed in this crystalline-state organorhodium system.

We are currently preparing various derivatives of dithionite complexes through chemical modification of the Cp* ligands in order to bring about new photoreaction dynamics by changing the reaction cavity and crystal packing.[17] Using our findings, it should be possible to prepare other functional molecular crystals.

## 4. Experimental Section

**Materials.** Solvents used were purified by distillation before use. Sodium dithionite, $Na_2S_2O_4$, was purchased form Aldrich. *trans*-$[(Cp^*Rh)_2(\mu\text{-}CH_2)_2Cl_2]$[10] was synthesized by using a published procedure. The deuterated dichlorodirhodium complex *trans*-$[(Cp^{*d15}Rh)_2(\mu\text{-}CH_2)_2Cl_2]$ was synthesized by using the same procedure as that for *trans*-$[(Cp^*Rh)_2(\mu\text{-}CH_2)_2Cl_2]$, but with deuterated *trans*-$[(Cp^{*d15}Rh)_2(\mu\text{-}Cl)_2Cl_2]$[18] as a starting material. All other chemicals were obtained from commercial sources and used as received unless otherwise noted.

**General Methods.** All experiments were performed under a dry nitrogen atmosphere using standard Schlenk techniques. $^1H$ and $^{13}C$ NMR spectra were recorded on JEOL Lambda 300 and 400 FT-NMR spectrometers in $CDCl_3$. Chemical shifts were referenced to *protio* solvent impurities ($^1H$: $\delta$ 7.26, $^{13}C$: $\delta$ 77.0 ($CDCl_3$)) and are reported in ppm. Infrared spectra were obtained as KBr pellets on a Jasco FT-IR-420 FT-IR spectrometer. Absorption spectra in solution were measured on a Jasco V-570 spectrophotometer. Absorption spectra of a microcrystalline powder film were measured by using a Leica DMLP polarizing microscope connected with a Hamamatsu PMA-11 photodetector. DSC analysis was performed using a Rigaku DSC-8230 differential scanning calorimeter. Elemental analyses were performed by the Analytical Research Service Center at Osaka City University on a Perkin-Elmer 240C elemental analyzer.

**Synthesis. $[(Cp^*Rh)_2(\mu\text{-}CH_2)_2(\mu\text{-}O_2SSO_2)]$ (1).** A mixture of *trans*-$[(Cp^*Rh)_2(\mu\text{-}CH_2)_2Cl_2]$ (200 mg, 0.29 mmol) and $Na_2S_2O_4$ (340 mg, 0.59 mmol) in MeOH (100 mL) was stirred for 4 h under $N_2$ in the dark at room temperature. The solvent was removed under reduced pressure to give a reddish brown solid. The crude product was dissolved in 50 mL of $CH_2Cl_2$, and the insoluble solid was filtered off. Removal of the solvent gave $[(Cp^*Rh)_2(\mu\text{-}CH_2)_2(\mu\text{-}O_2SSO_2)]$ (**1**) as a brown solid. The solid was washed with toluene and $Et_2O$. Yield 270 mg, 72%. Single crystals suitable for X-ray diffraction analysis were obtained by diffusion of AcOEt into a solution of **1** in $CH_2Cl_2$ at room temperature. $^1H$ NMR (400 MHz, $CDCl_3$): $\delta$ 9.47 (2H, s, $\mu$-$CH_2$), 8.53 (2H, s, $\mu$-$CH_2$), 1.85 (30H, s, $C_5Me_5$). $^{13}C$ NMR (100 MHz, $CDCl_3$): $\delta$ 174.2 ($\mu$-$CH_2$), 104.1 ($C_5Me_5$), 9.6 ($C_5Me_5$). Anal. calcd for $[(Cp^*Rh)_2(\mu\text{-}CH_2)_2(\mu\text{-}O_2SSO_2)]$: C, 41.78; H, 5.42%. Found: C, 41.68; H, 5.47%.

**$[(Cp^*Rh)_2(\mu\text{-}CH_2)_2(\mu\text{-}O_2SOSO)]$ (2).** Complex **2** can be synthesized by following two methods. Method A: Crystals of **1** were irradiated with xenon light (Asahi Spectra Co.,Ltd. MAX-320 with VIS mirror module: 300 W, 385−740 nm) for 3 h under $N_2$ at room temperature to yield crystals of complex **2**.

Method B: A suspension of **1** (200 mg, 0.32 mmol) in toluene (100 mL) was rapidly stirred and irradiated with fluorescent light (15 W, $\lambda_{max}$ = 545 nm) for 3 days at room temperature. Removal of the solvent gave $[(Cp^*Rh)_2(\mu\text{-}CH_2)_2(\mu\text{-}O_2SOSO)]$ (**2**) as an orange solid. This solid was washed with toluene and water. Yield 130 mg, 65%. Crystals of **2** suitable for X-ray diffraction analysis were grown from a saturated solution of MeOH at room temperature. All spectroscopic data were identical with those of the product obtained by method A. $^1H$ NMR (400 MHz, $CDCl_3$): $\delta$ 9.51 (1H, s, $\mu$-$CH_2$), 8.98 (1H, s, $\mu$-$CH_2$), 8.63 (1H, s, $\mu$-$CH_2$), 8.08 (1H, s, $\mu$-$CH_2$), 1.84 (15H, s, $C_5Me_5$), 1.75 (15H, s, $C_5Me_5$). $^{13}C$ NMR (100 MHz, $CDCl_3$): $\delta$ 178.5 ($\mu$-$CH_2$), 169.3 ($\mu$-$CH_2$), 104.9 ($C_5Me_5$), 104.7 ($C_5Me_5$), 9.7 ($C_5Me_5$), 9.3 ($C_5Me_5$). Anal. calcd for $[(Cp^*Rh)_2(\mu\text{-}CH_2)_2(\mu\text{-}O_2SOSO)]$: C, 41.78; H, 5.42%. Found: C, 41.76; H, 5.39%.

**$[(Cp^{*d15}Rh)_2(\mu\text{-}CH_2)_2(\mu\text{-}O_2SSO_2)]$ (1-$d_{30}$).** The procedure was exactly the same described above to prepare **1** using deuterated *trans*-$[(Cp^{*d15}Rh)_2(\mu\text{-}CH_2)_2Cl_2]$. The deuterium content of the $Cp^{*d15}$ in **1**-$d_{30}$ was 94% (estimated by $^1H$ NMR). $^1H$ NMR (400 MHz, $CDCl_3$): $\delta$ 9.49 (2H, s, $\mu$-$CH_2$), 8.55 (2H, s, $\mu$-$CH_2$), 1.85 (2H, m, $C_5Me_5$).

**$[(Cp^{*d15}Rh)_2(\mu\text{-}CH_2)_2(\mu\text{-}O_2SOSO)]$ (2-$d_{30}$).** Complexe **2**-$d_{30}$ was obtained by the same procedure described above to prepare **2** using **1**-$d_{30}$. The deuterium content of the $Cp^{*d15}$ in **2**-$d_{30}$ was 94% (estimated by $^1H$ NMR). $^1H$ NMR (400 MHz, $CDCl_3$): $\delta$ 9.53 (1H, s, $\mu$-$CH_2$), 9.00 (1H, s, $\mu$-$CH_2$), 8.64 (1H, s, $\mu$-$CH_2$), 8.10 (1H, s, $\mu$-$CH_2$), 1.81 (1H, m, $C_5Me_5$), 1.72 (1H, m, $C_5Me_5$).

**Computational Methods.** All the calculations were carried out using the Gaussian03 program package.

**Evaluation of the UV−vis Absorption Spectra of 1 and 2.** Vertical excitation energies and corresponding oscillator strengths for the lowest singlet excitation of **1** and **2** were calculated by using a time-dependent density functional theory (TD-DFT) method[19a−c] with the B3LYP functional.[19d] These calculations were performed on the ground-state structures determined by fixing the Rh−Rh, Rh−S, and S−S distances in **1** and the Rh−Rh, Rh−S, and S−O distances in **2** to the experimental distances (Figure 2), because the excitation energies should be sensitive to those bond distances. In order to determine the geometry, the LanL2DZ basis functions and effective core potential for Rh, 6−31G(d) for S and O, and 6−31G for C and H (basis set I) were used, and in TD-DFT calculations, the f polarization function was added to LanL2DZ on

(17) (a) Miyano, Y.; Nakai, H.; Hayashi, Y.; Isobe, K. *J. Organomet. Chem.* **2007**, *692*, 122–128. (b) Miyano, Y.; Nakai, H.; Mizuno, M.; Isobe, K. *Chem. Lett.* **2008**, *37*, 826–827.

(18) Kang, J. W.; Maitlis, P. M. *J. Organomet. Chem.* **1971**, *30*, 127–133.

(19) (a) Stratmann, R. E.; Scuseria, G. E.; Frisch, M. J. *J. Chem. Phys.* **1998**, *109*, 8218–8224. (b) Bauernschmitt, R.; Ahlrichs, R. *Chem. Phys. Lett.* **1996**, *256*, 454–464. (c) Casida, M. E.; Jamorski, C.; Casida, K. C.; Salahub, D. R. *J. Chem. Phys.* **1998**, *108*, 4439–4449. (d) Becke, A. D. *J. Chem. Phys.* **1993**, *98*, 5648–5652.

(20) (a) Ditchfield, R.; Hehre, W. J.; Pople, J. A. *J. Chem. Phys.* **1971**, *54*, 724–728. (b) Hehre, W. J.; Ditchfield, R.; Pople, J. A. *J. Chem. Phys.* **1972**, *56*, 2257–2261. (c) Hariharan, P. C.; Pople, J. A. *Theo. Chim. Acta* **1973**, *28*, 213–222. (d) Francl, M. M.; Pietro, W. J.; Hehre, W. J.; Binkley, J. S.; Gordon, M. S.; DeFrees, D. J.; Pople, J. A. *J. Chem. Phys.* **1982**, *77*, 3654–3665. (e) McLean, A. D.; Chandler, G. S. *J. Chem. Phys.* **1980**, *72*, 5639–5648. (f) Krishnan, R.; Binkley, J. S.; Seeger, R.; Pople, J. A. *J. Chem. Phys.* **1980**, *72*, 650–654. (g) Frisch, M. J.; Pople, J. A.; Binkley, J. S. *J. Chem. Phys.* **1984**, *80*, 3265–3269. (h) Clark, T.; Chandrasekhar, J.; Spitznagel, G. W.; Schleyer, P. V. R. *J. Comput. Chem.* **1983**, *4*, 294–301. (i) Hay, P. J.; Wadt, W. R. *J. Chem. Phys.* **1985**, *82*, 299–310. (j) Ehlers, A. W.; Böhme, M.; Dapprich, S.; Gobbi, A.; Höllwarth, A.; Jonas, V.; Köhler, K. F.; Stegmann, R.; Veldkamp, A.; Frenking, G. *Chem. Phys. Lett.* **1993**, *208*, 111–114.

Rh. In addition, 6−311+G(3df) and &-31G(d) were used on S and O and C and H (basis set II), respectively.[20]

**Energy Calculations for *trans*- and *cis*-isomers of 2.** The structures were fully determined using the B3LYP/I method. To obtain more reliable energetics, energy calculations for the structures thus determined were performed at the B3LYP/II level. These calculations showed that the *trans*-isomer was 2.3 kcal/mol more stable than the *cis*-isomer. Zero-point vibrational energy corrections caused a decrease of 0.3 kcal/mol in the energy difference.

**Crystallography.** X-ray crystallographic analysis was carried out using a Rigaku RAXIS-RAPID Imaging Plate diffractometer with Mo Kα radiation ($\lambda$ = 0.71073 Å). Crystal data for **1**: $C_{22}H_{34}O_4Rh_2S_2$, MW = 632.44, monoclinic, space group $P2_1/n$, $Z$ = 4, $T$ = 100 K, $a$ = 8.394(2) Å, $b$ = 36.532(8) Å, $c$ = 8.430(2) Å, $\beta$ = 116.213(10)°, $V$ = 2319.2(10) Å$^3$, goodness of fit = 1.024, $R1[I > 2\sigma(I)]$ = 0.0567, $wR2$(all data) = 0.1039. Crystal data for **2**: $C_{22}H_{34}O_4Rh_2S_2$, MW = 632.44, monoclinic, space group $P2_1/n$, $Z$ = 4, $T$ = 100 K, $a$ = 8.339(2) Å, $b$ = 36.750(9) Å, $c$ = 8.447(2) Å, $\beta$ = 115.594(10)°, $V$ = 2334(1) Å$^3$, goodness of fit = 1.039, $R1[I > 2\sigma(I)]$ = 0.0650, $wR2$(all data) = 0.1365. Crystallographic data were deposited with the Cambridge Crystallographic Database Centre (**1**: CCDC-603301; **2**: CCDC-603302). The following crystallographic data are in the Supporting Information (data at 2 h, 18 h, and 132 h in Figure 6a: f6a_2h.cif, f6a_18h.cif, and f6a_132h.cif, respectively; data at 8 h, 46 h, and 190 h in Figure 6b: f6b_8h.cif, f6b_46h.cif, and f6b_190h.cif, respectively; data at 12 and 84 h in Figure 8: f8_12h.cif and f8_84h.cif, respectively).

Positional disorder of oxygen atoms during the photoreaction was treated with as follows: the sum of experimental occupancies O1, O3, and O5 and O2, O4, and O6 was always nearly 2.0 in the middle stage of the reaction, which means that the no *cis*-isomer (Figure 7) was present. Thus, refinement of the occupancies was done by assuming that only **1** and **2** with four *trans* orientations, as shown in Figure 5, were present in the single crystals giving the sums of occupancies of O1, O3, and O5 and O2, O4, and O6 of 2.000(5). Although the positions of the sulfur atoms in the single crystals were also disordered, the peaks of the electron density for the disordered atoms were too close to treat them as separated atoms. However, the S−S distances were used to determine the mixing rate of **1** and **2**.

**Solid-State NMR Spectroscopy.** Solid-state NMR spectra were acquired on a Chemagnetics CMX-300 spectrometer operating at 75.05 and 45.818 MHz for $^{13}$C and $^2$H, respectively. The $^{13}$C CP/MAS NMR spectra were acquired in a 7.5 mm probe with 80 − 100 mg of sample and a spinning rate of 3 kHz. An optimum contact time of 1 ms was determined at ambient temperature, and the same value was used for other temperature measurements. The total suppression of side bands (TOSS) sequence was used to suppress spinning side bands. Lineshape simulations were carried out using a home-written FORTRAN program assuming a five-site jump of the Cp* ring around the $C_5$-axis.[21]

$^2$H spectra were obtained with 80 − 100 mg of sample in a 5 × 20 mm glass tube. The spectra were acquired in a 6 mm probe using a quadrupolar echo pulse sequence ($90°_x-\tau-90°_y-\tau$). The 90° pulse width was typically 2−3 $\mu$s, and the delay time $\tau$ was set to 20 $\mu$s. Spectra were fitted using a home-written FORTRAN program with $e^2Qq/h$ = 50 kHz and $\eta$ = 0.

**Acknowledgment.** This work was financially supported by the Grant-in-Aids for Scientific Research (KAKENHI) in Priority Areas "Chemistry of Coordination Space", "Synergy of Elements", and "Photochromism" and by the Grant-in-Aids "15350036" and "1635002" from Ministry of Education, Culture, Sports, Science and Technology (MEXT), Japan. Part of the calculations was carried out at the Research Center for Computational Science, Okazaki, Japan (This research was supported by CREST, JST). We thank Prof. Brian K. Breedlove for his helpful remarks concerning our paper.

**Supporting Information Available:** Complete ref 12 and crystallographic data. This material is available free of charge via the Internet at http://pubs.acs.org.

JA807150A

(21) Steigel, A. *Dynamic NMR spectroscopy: NMR basic principles and Progress*; Springer: Berlin, 1978; Vol. 15, pp 1−54.